# Does source complexity govern tsunami generation?

Fabian Kutschera[1]* & Alice-Agnes Gabriel[1,2]

1 Institute of Geophysics and Planetary Physics, Scripps Institution of Oceanography, University of California San Diego, USA; 2 Department of Earth and Environmental Sciences, Ludwig-Maximilians-University Munich, Germany

*Email: fkutschera@ucsd.edu

## Motivation

Understanding the complex dynamics of earthquake-tsunami interaction is essential for both tsunami early warning and for self-consistent modeling. Earthquake and tsunami hazard assessments are also often conducted separately, while tsunamigenic earthquakes pose considerable risks, both economically and socially.

Here, we show three case studies of joint earthquake-tsunami modeling:

(1) Kinematically constrained, linked and fully coupled dynamic rupture and tsunami modeling of the 2020, $M_W$ 7.0 Samos Earthquake.

(2) Linked and fully coupled 3D strike-slip earthquake dynamic rupture and tsunami modeling for the Húsavík-Flatey Fault Zone in North Iceland.

(3) A complex multi-fault uplift model for the 2024, $M_W$ 7.5 Noto Peninsula earthquake, obtained through a multiple centroid moment tensor Bayesian inversion of seismic data, and how it can be used for tsunami modeling.

## (1) The 2020 $M_W$ 7.0 normal faulting Samos earthquake

We aim to unravel the complexity of rupture and tsunami generation by comparing kinematic source models with kinematically informed 3D dynamic rupture models and using different tsunami modeling techniques.

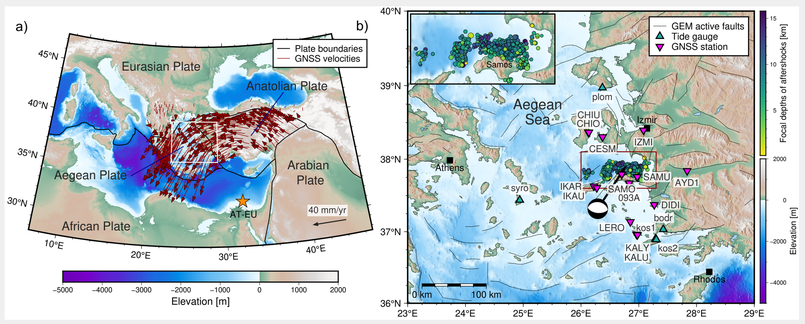


**Fig 1 a) Tectonic setting** with present-day circular counterclockwise kinematic motion of regional GNSS stations. **b) Aegean Sea region** and location of the Samos earthquake, which activated an east-west striking normal fault [e.g., 7, 8].

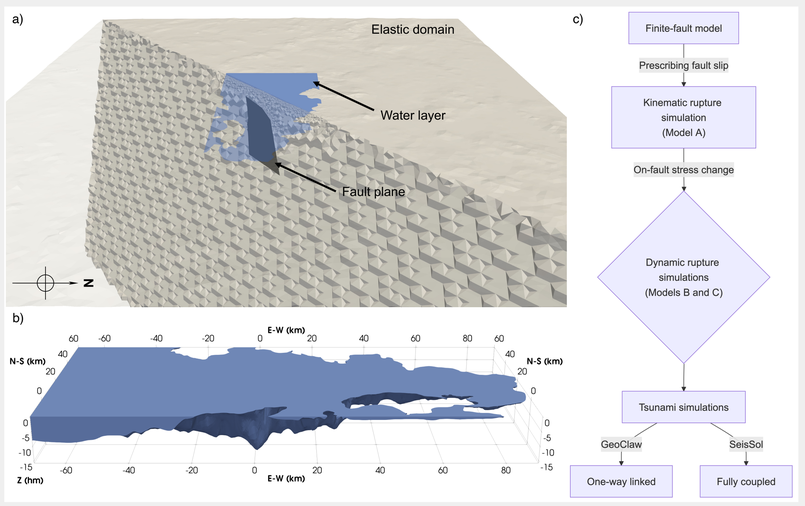


**Fig 2 a) Transection of the three-dimensional unstructured tetrahedral mesh**. **b) Dimension of the water layer**. Here, we prescribe a rigidity of $\mu = 0$ [3,4]. **c) Workflow of this study**, which may help to design and guide rapid workflows for the joint assessment of physics-based seismic and tsunami hazards. We start with a finite-fault model [7] and prescribe its slip distribution in a kinematic rupture model.

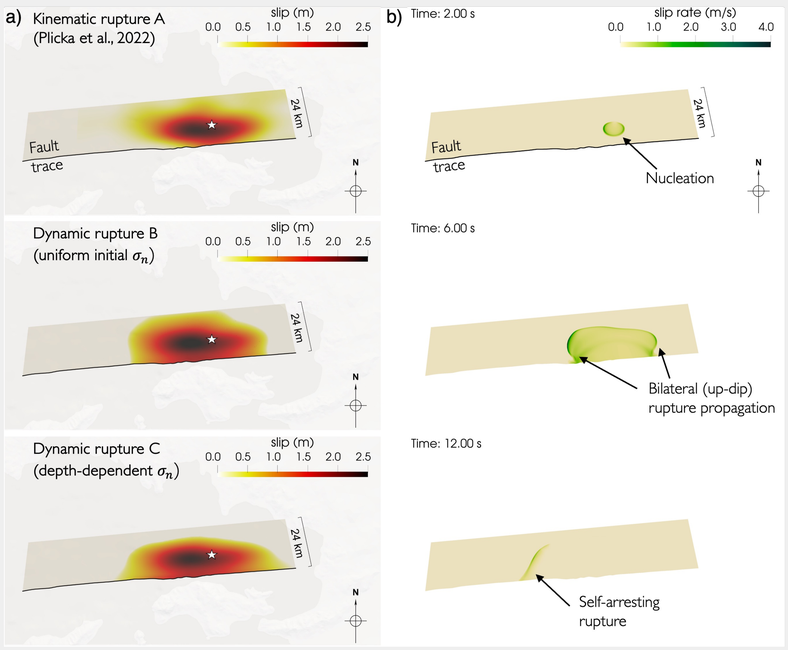


**Fig 3 a) Final slip distributions** of selected models. Shear stress changes in dip direction of Model A informs two spontaneous dynamic rupture models [9]: models with uniform and depth-dependent initial normal stress generate comparable peak slip amplitudes. **b) Spontaneous spatio-temporal rupture evolution** of Model C featuring a bilateral up-dip rupture propagation and self-arresting rupture.

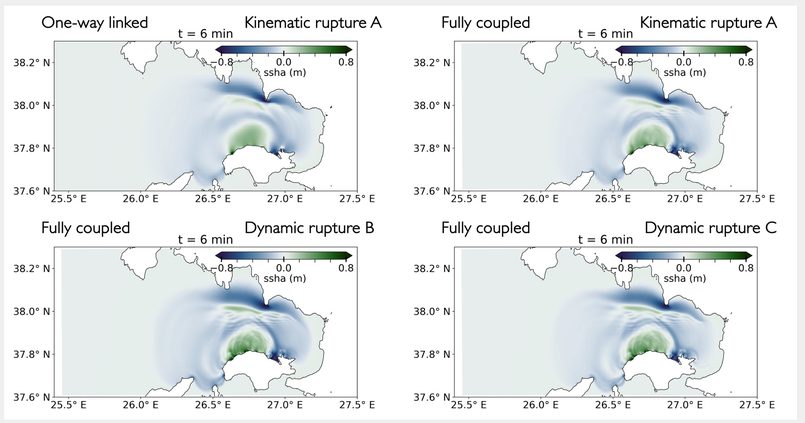


**Fig 4 Tsunami simulations sourced by time-dependent forcing** using non-linear shallow water equations (GeoClaw) and the fully coupled earthquake-tsunami modeling technique (SeisSol) [1,3,4]. The tsunami synthetics of the more complex fully coupled earthquake-tsunami simulations contain a higher frequency content than the "smoother" one-way linked tsunami waveforms.

- **Wave depression of up to 2 m** in Kuşadası Bay is accompanied by max. tsunami amplitudes of up to 1 m.

## (2) Strike-slip dynamic rupture and tsunami modeling

We present a **suite of realistic 3D dynamic rupture earthquake-tsunami scenarios** for the Húsavík-Flatey Fault Zone in North Iceland and compare one-way linked and fully coupled modeling workflows on two fault system geometries. The dynamic rupture simulation on a less segmented strike-slip fault system causes local tsunami wave heights (crest to trough) of up to ~0.9 m due to the large shallow fault slip (~8 m), **rake rotation (± 20°)**, and coseismic vertical displacements (± 1 m).

Kutschera et al. (2024a)

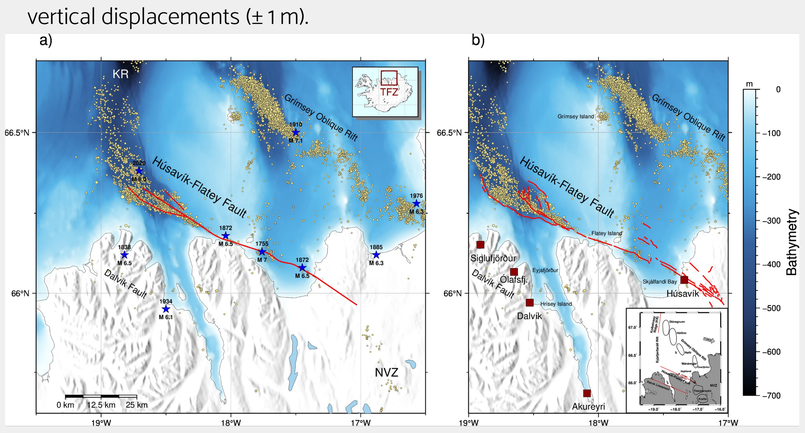


**Fig 5** Overview of the Tjörnes Fracture Zone (TFZ), which connects the Kolbeinsey Ridge (KR) as part of the Mid-Atlantic Ridge offshore north of Iceland to its manifestation on land in the Northern Volcanic Zone (NVZ). (a) The "simple" **fault geometry of the Húsavík-Flatey Fault Zone (HFFZ)**, which has three segments, shown as red lines [6]. **Historic large earthquakes** with M≥6 are indicated as blue stars. (b) The "complex" fault geometry of the HFFZ [6], which includes 55 fault segments.

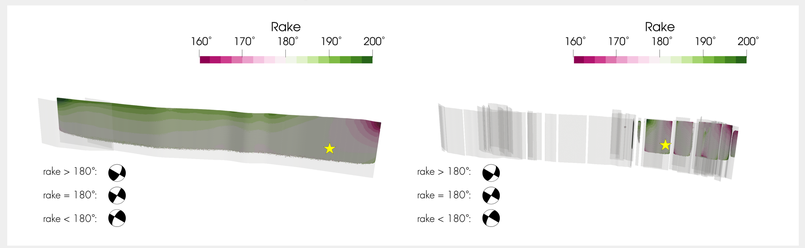


**Fig 6 Dynamic rake rotation near the surface** in the dynamic rupture simulations on (a) the simple fault geometry and (b) the complex fault geometry. Yellow stars mark the hypocenter locations. A rake of 180° indicates pure right-lateral strike-slip faulting.

- The dynamic deviations from pure right-lateral strike-slip faulting are on the order of ± 20° and **introduce significant shallow dip-slip motion**. Thereby, vertical seafloor displacements in our simulations are enhanced, which are critical for tsunami generation.
- Shallow rake rotation has been inferred for surface-breaking earthquakes using geological slickenlines and simple dynamic rupture models [e.g., 2].
- Vertical stress changes at the rupture front cause this change in rake angle, which is more pronounced near the surface due to smaller confining stresses.

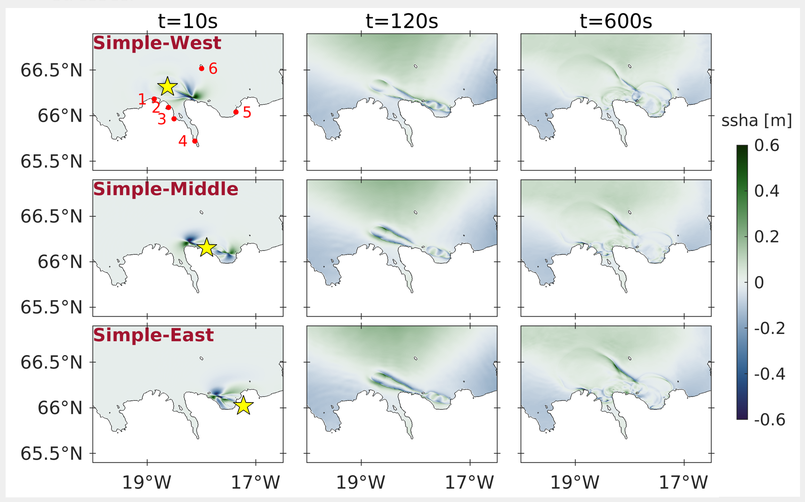


**Fig 7 Sea surface height anomaly (ssha) of one-way linked earthquake-tsunami scenarios** at 10 s (first column), 2 min (second column), and 10 min (third column) simulation times. The yellow star in the first column marks the epicenter of each scenario. The red points in the top-left panel indicate the position of synthetic tide gauges near local coastal towns.

- **Strike-slip earthquakes can produce sizeable (local) tsunami**
- Fully coupled earthquake-tsunami models indicate **unexpectedly large acoustic waves** compared to tsunami signals:
  - i. May serve as a rapid indicator of surface-breaking dynamic rupture.
  - ii. Complicate the detection of tsunami signal in tsunami early warning.

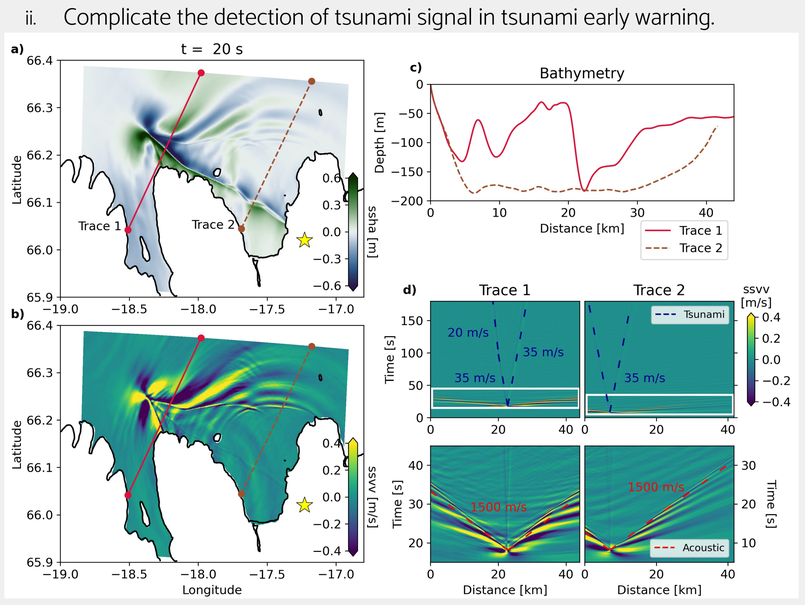


**Fig 8** The **3D fully coupled earthquake-tsunami scenario** Simple-East, with dynamic rupture on the simple fault geometry and a hypocenter in the east (yellow star). Snapshots at t = 20 s of (a) the sea surface height anomalies (ssha) and (b) sea surface vertical velocity (ssvv). (c) Bathymetry profiles. (d) Space–time evolution of ssvv along the two cross sections for the full duration of the fully coupled simulations (upper row: highlighting the tsunami; lower row: highlighting the fast-propagating acoustic waves).

## (3) Using multi-CMT solutions for tsunami modeling

We present tsunami models informed by a 6-subevent centroid moment tensor (CMT) model obtained through Bayesian inversion of teleseismic and strong motion data for the 2024, $M_W$ 7.5 Noto Peninsula earthquake. We identify **two distinct bilateral rupture episodes**. Initial, onshore rupture toward the southwest is followed by **delayed re-nucleation** at the hypocenter, likely aided by fault weakening, causing significant seafloor uplift to the northeast. We construct a **complex multi-fault uplift model**, validated against geodetic observations, that aligns with known fault system geometries and is **critical in modeling the observed tsunami**. The simulations can explain tsunami wave amplitude, timing, and polarity of the leading wave, which are crucial for tsunami early warning.

Kutschera et al. (2024b)

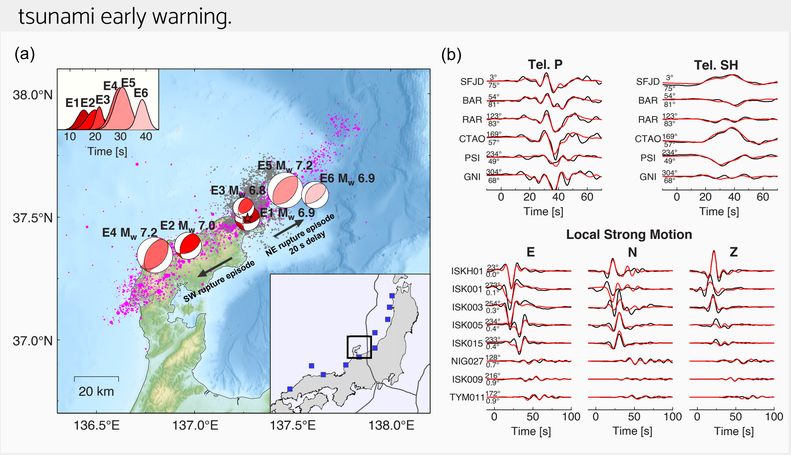


**Fig 9 (a) Overview of the Noto Peninsula, Japan**. The red focal mechanisms are the six subevents of the **Bayesian multi-centroid moment tensor (CMT) inversion** using teleseismic and regional strong motion data. (b) Comparison of selected observed (black) teleseismic P, SH (both in displacement), and local strong ground motion recordings (in velocity) with the corresponding synthetic seismic waveforms (red) of the preferred multi-CMT solution.

- The earthquake first initiates toward the southwest, indicated by subevents E1, E2, and E4. After a delay of 20 s, the rupture unfolds toward the northeast, as indicated by subevents E3, E5, and E6.

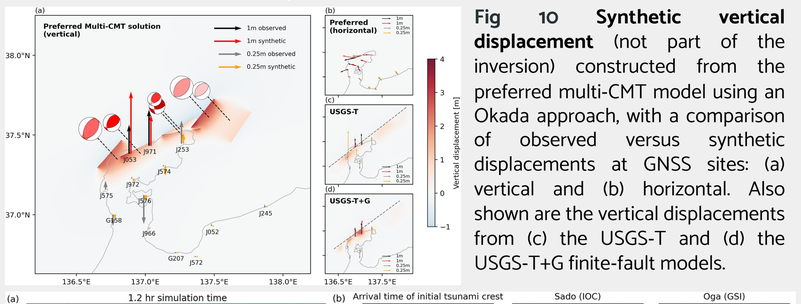


**Fig 10 Synthetic vertical displacement** (not part of the inversion) constructed from the preferred multi-CMT model using an Okada approach, with a comparison of observed versus synthetic displacements at GNSS sites: (a) vertical and (b) horizontal. Also shown are the vertical displacements from (c) the USGS-T and (d) the USGS-T+G finite-fault models.

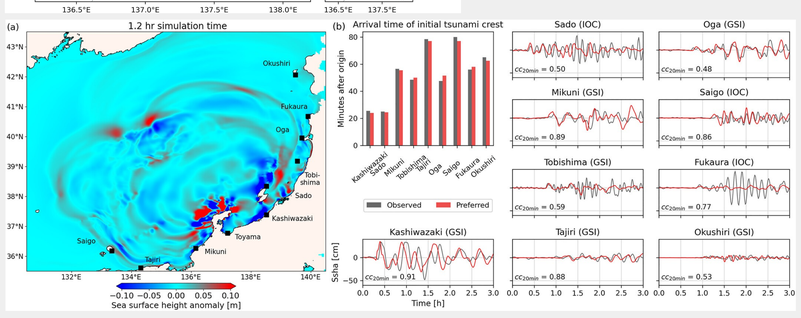


**Fig 11** (a) Snapshot of tsunami propagation 1 hr and 12 min after the earthquake origin time, showing **strong tsunami reverberations** surrounding the Noto Peninsula. (b) Comparison of observed and simulated tsunami arrival times, along with a comparison of tsunami waveforms at nine tide gauges.

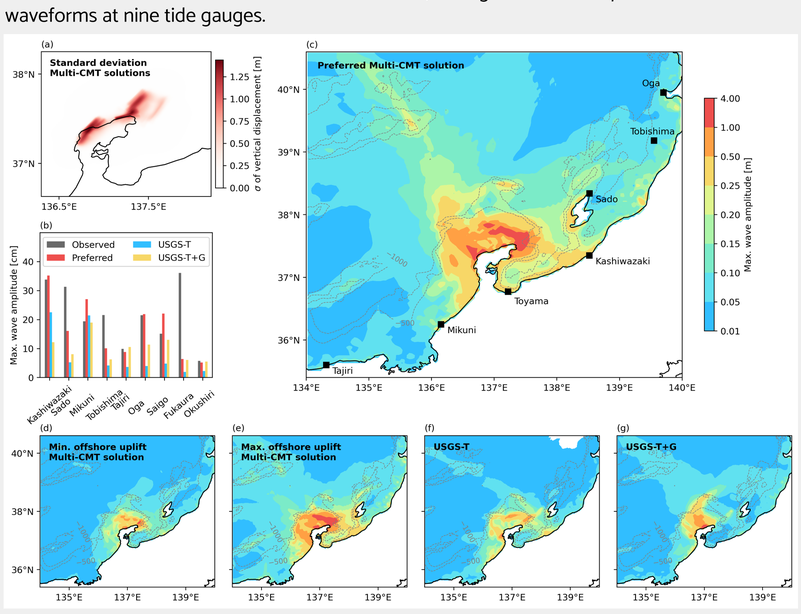


**Fig 12** (a) Standard deviation of the vertical displacements based on an ensemble of 2000 multi-CMT solutions. (b) Histogram of the observed and simulated maximum wave amplitudes over a 3 hr time window after the earthquake's origin time at the tide gauge locations. (c-g) **Tsunami maximum wave amplitude distributions**.

## Conclusions

- Tsunami simulations for the 2020, $M_W$ 7.0 Samos normal faulting earthquake indicate fully coupled dynamic rupture simulations yield the most complex tsunami excitation.
- Strike-slip earthquakes can generate local tsunamis as shown by a case study for the ~100 km long Húsavík–Flatey Fault Zone in North Iceland.
- Analysis of 2000 multi-CMT solutions and of alternative source models for the 2024, $M_W$ 7.5 Noto Peninsula reverse faulting earthquake shows complex source effects are important for realistic tsunami models.

Selected references:

[1] Abrahams, L. S., Krenz, L., Dunham, E. M., Gabriel, A.-A. & Saito, T. Comparison of methods for coupled earthquake and tsunami modelling. Geophysical Journal International 234, 404–426 (2023).

[2] Kearse, J., Kaneko, Y., Little, T. & Van Dissen, R. Curved slickenlines preserve direction of rupture propagation. Geology 47, 838–842 (2019).

[3] Krenz, L. et al. 3D Acoustic-Elastic Coupling with Gravity: The Dynamics of the 2018 Palu, Sulawesi Earthquake and Tsunami. International Conference for High Performance Computing, Networking, Storage and Analysis, SC (2021)

[4] Kutschera, F. et al. Linked and fully coupled 3D earthquake dynamic rupture and tsunami modeling for the Húsavík–Flatey Fault Zone in North Iceland. Solid Earth 15, 251–280 (2024a).

[5] Kutschera, F. et al. The Multi-Segment Complexity of the 2024 Mw 7.5 Noto Peninsula Earthquake Governs Tsunami Generation. Geophysical Research Letters 51, e2024GL109790 (2024b).

[6] Li, B., Gabriel, A.-A., Ulrich, T., Abril, C. & Halldorsson, B. Dynamic Rupture Models, Fault Interaction and Ground Motion Simulations for the Segmented Húsavik-Flatey Fault Zone, Northern Iceland. Journal of Geophysical Research: Solid Earth 128, e2022JB025886 (2023).

[7]Plicka, V. et al. The 2020 Samos Mw7 earthquake: Source model depicting complexity and rupture directivity. Tectonophysics 843 (2022).

[8] Sun, Y.-S. et al. The 2020 Mw 7.0 Samos (Eastern Aegean Sea) Earthquake: joint source inversion of multitype data, and tsunami modelling. Geophysical Journal International 237, 1285–1300 (2024).

[9] Tinti, E. et al. Constraining families of dynamic models using geological, geodetic and strong ground motion data: The Mw 6.5, October 30th, 2016, Norcia earthquake, Italy. Earth and Planetary Science Letters 576, 117237 (2021).

Homepage

Scan me!